CHEMISTRY OF MATERIALS

ARTICLE

pubs.acs.org/cm

Preparation of Tunable 3D Pillared Carbon Nanotube–Graphene Networks for High-Performance Capacitance

Feng Du,[†,§] Dingshan Yu,[†,§] Liming Dai,[†,*] S. Ganguli,[‡] V. Varshney,[‡] and A. K. Roy[‡,*]

[†]Center of Advanced Science and Engineering for Carbon (Case4Carbon), Department of Macromolecular Science and Engineering, Case Western Reserve University, Cleveland, Ohio 44106, United States

[‡]Thermal Sciences and Materials Branch, Materials & Manufacturing Directorate, Air Force Research Laboratory, Dayton, Ohio 45433, United States

Supporting Information

ABSTRACT: We have developed a rational strategy for creating the 3D pillared vertically aligned carbon nanotube (VACNT)-graphene architectures by intercalated growth of VACNTs into thermally expanded highly ordered pyrolytic graphite (HOPG). By controlling the fabrication process, the length of the VACNT pillars can be tuned. In conjunction with the electrodeposition of nickel hydroxide to introduce the pseudocapacitance, these 3D pillared VACNT–graphene architectures with a controllable nanotube length were demonstrated to show a high specific capacitance and remarkable rate capability, and they significantly outperformed many electrode materials currently used in the state-of-the-art supercapacitors.

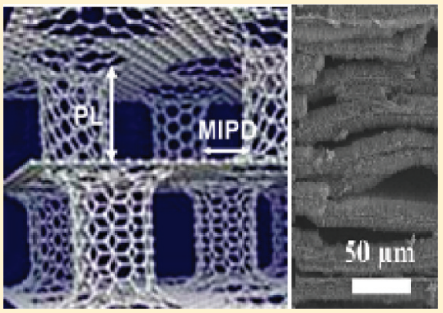

KEYWORDS: carbon nanotube, graphene, 3D pillared VACNT–graphene, nickel hydroxide, supercapacitors

INTRODUCTION

Carbon nanomaterials, including one-dimensional (1D) carbon nanotubes (CNTs) and two-dimensional (2D) single-atomic layer graphene, have been demonstrated to show superior thermal, electrical, and mechanical properties attractive for a wide range of potential applications.[1−12] Carbon nanomaterials have made a big impact on energy generation and storage by offering new materials/systems with unique architectures and properties.[13,14] As a result of the presence of strong covalent bonding in the carbon plane and the much weaker van der Waals interaction in the transverse direction between the layers, however, CNTs and graphene exhibit strong direction-dependent thermal and electrical transport properties with extremely low out-of-plane conductivities. Theoretical studies[15−19] have indicated that 3D pillared architectures, consisting of parallel graphene layers supported by vertically aligned carbon nanotubes (VACNTs) in between, possess desirable out-of-plane transport and mechanical properties while maintaining the excellent properties of their building blocks. Of particular interest, computer modeling has predicted that such a 3D pillared VACNT–graphene structure can be used for efficient hydrogen storage after being doped with lithium cations.[16] Theoretical studies carried out by Roy and co-workers[15] indicate that thermal transport properties of the 3D pillared VACNT–graphene structure are governed by the minimum interpillar distance (MIPD) and the CNT-pillar length (PL) (Figure 1a). Some successes in fabricating randomly oriented CNT/graphene sandwiches[20−22] or a single layer of VACNTs on a graphene substrate[23] have been reported. Regardless of the great theoretical and experimental interest and tremendous scientific and technological potential of these nanostructures, however, no such 3D pillared VACNT–graphene architecture has been experimentally realized to date as a result of technical difficulties. Once fabricated, these inherently nanoporous 3D pillared VACNT–graphene architectures with large surface areas should allow for tunable thermal, mechanical, and electrical properties, which would be useful in many potential applications, including advanced supercapacitors.

The objective of this study is to develop a rational strategy for the extension of the unique properties of CNTs and graphene to the critical third dimension. On the basis of our previous work on the growth of VACNTs by the pyrolysis of iron phthalocyanine (FePc),[24] we have created tunable 3D pillared VACNT–graphene architectures through intercalated growth of VACNTs into thermally expanded highly ordered pyrolytic graphite (HOPG) by the pyrolysis of FePc.[24] Although the graphitic layers achieved in these pillared nanostructures were not always to be single layer graphene sheets (designated as: graphene for convenience), these 3D pillared VACNT–graphene nanostructures with a controllable nanotube length (PL)/intertube distance (MIPD) were demonstrated to be excellent electrode materials for energy-related devices. In conjunction with the electrodeposition of nickel hydroxide to introduce the pseudocapacitance, the resultant hybrid materials significantly outperformed many electrode materials, including RuO_2,[25] MnO_2,[26] NiO,[27] Mn_3O_4,[28] and $Ni(OH)_2$[29,30] as well as their composites with CNTs or graphene,[31−36] currently used in the state-of-the-art supercapacitors. Here, we report the fabrication of tunable 3D

Received: July 24, 2011
Revised: September 23, 2011
Published: October 17, 2011

pillared VACNT−graphene architectures by the first intercalated growth of VACNTs into thermally expanded highly ordered pyrolytic graphite (HOPG) for supercapacitor applications.

RESULTS AND DISCUSSION

Figure 1b schematically shows the procedure for creating the 3D pillared VACNT−graphene architectures. In a typical experiment, a piece of HOPG was first immersed into a mixture of sulfuric and nitric acids (3:1 v/v) for 10 min at room temperature with sonication in a water bath (step 1, Figure 1b). Subsequent heating of the acid-treated HOPG up to 900 °C in Ar caused the thermal vaporization of the acid molecules physically trapped between the graphene layers, leading to a dramatic expansion along the graphite *c*-axis[37] (step 2, Figure 1b). The thermally expanded HOPG was then treated in a tube furnace at 1000−1200 °C under purging gas mixture flow of Ar (300 SCCM) and H_2 (30 SCCM) bubbling through silicon tetrachloride ($SiCl_4$) in an ambient atmosphere to produce the SiO_2 coating for facilitating the growth of VACNTs[38] (step 3, Figure 1b). As demonstrated by our previous work,[38] the SiO_2 coating is needed to ensure uniform growth of VACNTs, which otherwise would be impossible due to the ill-defined catalyst particle formation associated with the surface tension mismatch. Finally, the 3D pillared VACNT−graphene architecture was produced by pyrolysis of FePc at 800−1000 °C under Ar/H_2 according to the published procedure[24] (step 4, Figure 1b). The resultant VACNT−graphene 3D networks showed a several fold increase in mass with a concomitant volume expansion of a few hundred times with respect to the original graphite (Figure 1c and d).

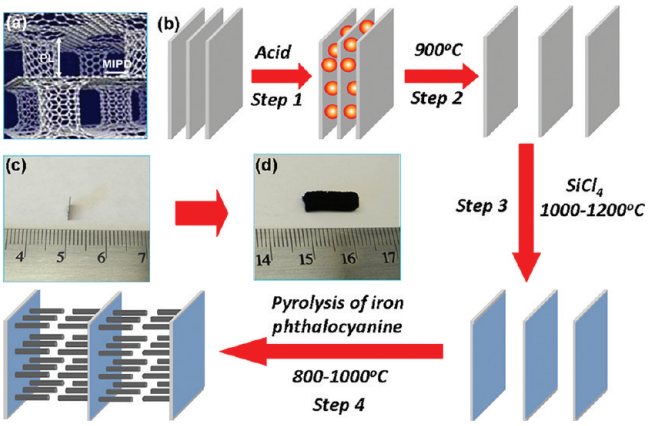

Figure 1. (a) Schematic diagram of a 3D pillared VACNT−graphene nanostructure. (b) Schematic representation of the procedure for the preparation of the 3D pillared VACNT−graphene architectures. Optical images of (c) original HOPG with a thickness of 80 μm and (d) the thermally expanded graphene layers intercalated with VACNTs.

Figure 2a−d shows scanning electron microscopy (SEM) images for the original HOPG, along with the acid-treated HOPG before and after the intercalated growth of VACNTs. The well-defined layered structure characteristic of the pristine HOPG is evident in Figure 2a. After the acid-treatment and thermal expansion (steps 1 and 2, Figure 1b), the layered structure was significantly expanded and somewhat distorted (Figure 2b). Subsequent coating with SiO_2 (step 3, Figure 1b)

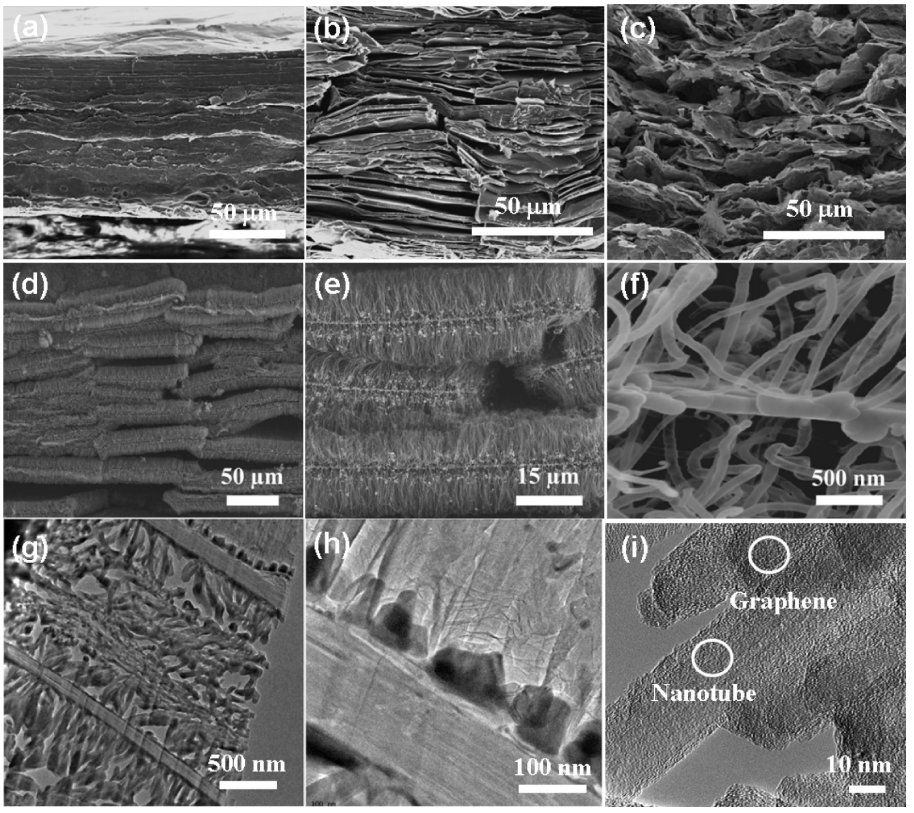

Figure 2. SEM images of (a) the pristine HOPG and the acid-treated, thermally expanded HOPG (b) without and (c) with SiO_2 coating. (d−f) Typical SEM images of the 3D pillared VACNT−graphene architectures under different magnifications. (g−i) Cross-sectional TEM images of the 3D pillared VACNT−graphene architectures under different magnifications.

dx.doi.org/10.1021/cm2021214 |*Chem. Mater.* 2011, 23, 4810–4816

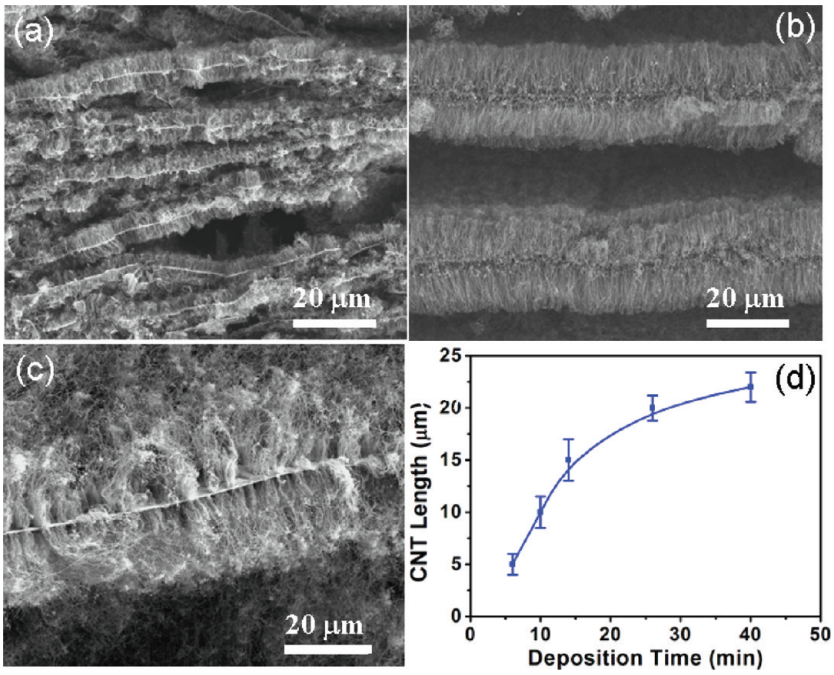

Figure 3. (a−c) SEM images of the thermally expanded graphene layers intercalated with VACNTs for different pyrolysis times of 5, 10, and 30 min, respectively, and (d) the VACNT pillar height as a function of the nanotube deposition time.

caused further interlayer expansion and structure distortion (Figure 2c).

Upon pyrolysis of FePc (step 4, Figure 1b), VACNTs were intercalated into the gaps between the thermally expanded graphene layers via the in situ growth process[24] (Figure 2d). The newly formed graphene-supported VACNT "forests" are clearly seen in Figure 2e under a higher magnification, which also shows that the VACNTs grew from both sides of adjacent graphene sheets in the thermally expanded HOPG, with an intimately contacted VACNT−graphene interface (Figure 2f). Transmission electron microscopy (TEM) images of the 3D pillared VACNT−graphene sample, after cutting through its cross section by a focused ion beam (FIB), given in Figure 2g and h show the feature similar to that shown in the corresponding SEM images, but with a clearer view of the iron catalyst particles at the VACNT−graphene interface (Figure 2h and Figure S1 in the Supporting Information) due to the "base-growth" process.[24] A higher magnification TEM image taken at the VACNT−graphene interface, given in Figure 2i, clearly shows that the lattice orientation in the nanotube matches well with that in the graphene layer; some of the aligned CNTs penetrated into the underlying graphite substrate.[38]

By varying the FePc pyrolysis time, we can tune the length of the VACNT pillars (PL). Figure 3a−c clearly shows that the length of the VACNT pillars increase with increasing the nanotube deposition time. The steady increase in the VACNT pillar length with the nanotube deposition time seen in Figure 3d indicates that the growing VACNT pillars are sufficiently strong to "push" the stacked graphene layers apart from each other. For the 3D pillared VACNT−graphene architecture intercalated with 20-μm long VACNT pillars (Figure 3c), a 200 times volume expansion and a 60% weight increase with respect to the original HOPG were observed.

We further used XRD to follow the acid-induced thermal expansion and subsequent intercalated growth of VACNTs. As expected, Figure 4A(a) shows two sharp peaks at $2\theta = 28.1°$ and 55.9°, respectively, which correspond to the (002) and (004) reflection of HOPG. The (002) and (004) peaks are indicative of perpendicular direction (c-axis) to the graphite hexagonal planes.[39] The thermal treatment caused a downshift for the (002) peak, which was accompanied by the appearance of a new broad band centered $2\theta = 18.5°$ and a significant intensity decrease for the (002) and (004) peaks (Figure 4A(b)). These changes imply the presence of expanded stacking regions of more corrugated (disordered) thinner graphene sheets.[39] After a prolonged acid-treatment (24 h), the peak at $2\theta = 19°$ for the thermally expanded graphite became dominate while the (002) and (004) peaks associated with the intergraphene sheet spacing were almost completely suppressed. This indicates an almost complete exfoliation of graphite,[40] leading to an inappropriate thermal expansion for the fabrication of the 3D pillared VACNT−graphene architectures.

The XRD patterns of the thermally expanded graphite (acid-treatment time of 30 min) intercalated with 5 to 10 μm long VACNTs (Figure 4A(d and e)) show the feature similar to that of the acid-treated starting material (Figure 4A(b)). When the intercalated VACNT pillar length increased to 20 μm (Figure 4A(f)), the broad peak at 19° increased significantly with respect to the sharp peak around 27°, indicating, once again, that the longer VACNT pillars have "pushed" the stacked graphene layers into a more disordered structure.[40] The observed intensity increase for the broad peak at 19° came from both the above-mentioned order−disorder transition of the thermally expanded graphite layers and the intercalation of VACNTs that also showed an XRD peak around 19°.

The structure changes caused by the thermal expansion and VACNT intercalation were further followed by Raman measurements. As can be seen in Figure 4B, the I_D/I_G ratio increases not only with increasing the acid-treatment time (Figure 4B(a−c)) as a result of the acid-treatment-induced disordered structures

dx.doi.org/10.1021/cm2021214 |*Chem. Mater.* 2011, 23, 4810–4816

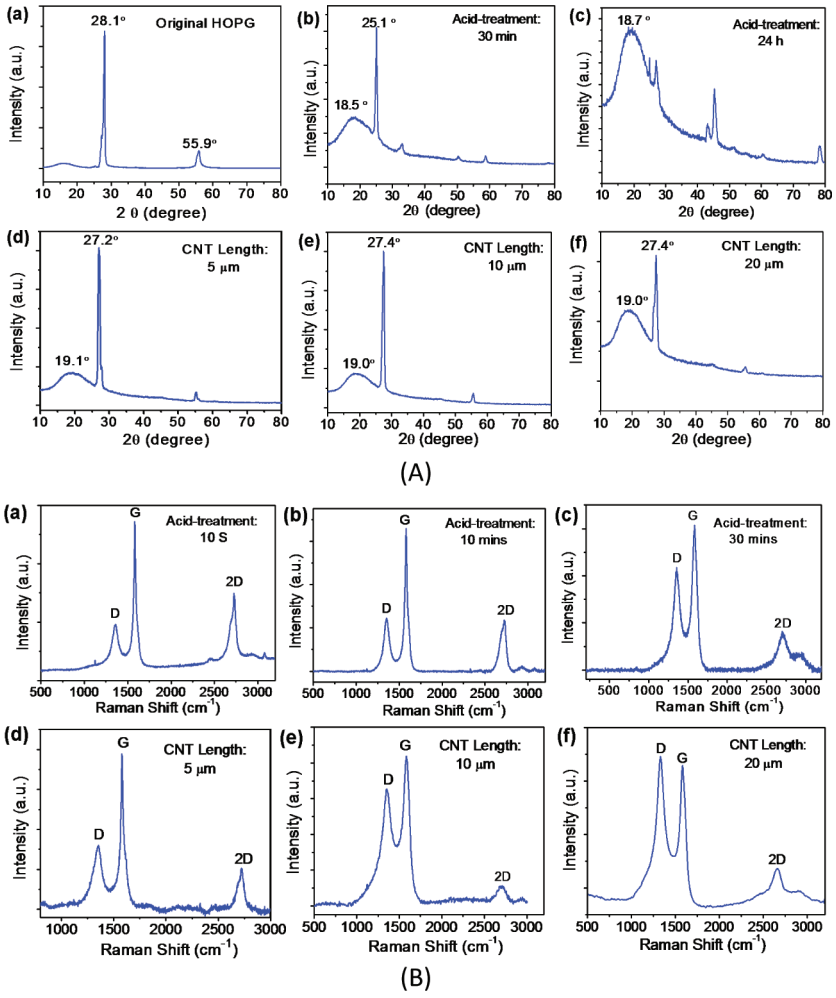

Figure 4. (A) XRD patterns of thermally expanded HOPGs with different times of acid treatment: (a) 0 min, (b) 30 min, and (c) 24 h. XRD patterns of thermally expanded HOPGs with the same acid-treatment time of 30 min after being intercalated with VACNTs of different nanotube lengths: (d) 5 μm, (e) 10 μm, and (f) 20 μm. (B) Raman spectra for the thermally expanded HOPG with the different acid treatment times: (a) 10 s, (b) 10 min, and (c) 30 min. Raman spectra for the thermally expanded HOPG intercalated with VACNTs of different nanotube lengths (at the same acid-treatment time of 10 min, cf. Figure 5b): (d) 5 μm, (e) 10 μm, and (f) 20 μm.

but also with the CNT pillar length in the VACNT−graphene hybrid architectures (Figures 4B(d−f)) as a result of the disordered graphene and CNT structures induced by the VACNT intercalation.

To demonstrate the porous nature of the 3D pillared VACNT−graphene architectures, we carried out the Brunauer−Emmett−Teller (BET) measurements. A BET surface area up to 213.7 ± 2.1 m^2/g was obtained based on nitrogen adsorption−desorption analyses (Figure S3a in the Supporting Information). Figure S3b in the Supporting Information shows a type-IV nitrogen adsorption isotherm for the 3D VACNT−graphene nanostructure (i.e., a mesoporous material according to the IUPAC classification) with a pore size in the range 1−12 nm. The pore size distribution was obtained from the corresponding pore volume distribution (Figure S3b in the Supporting Information) by assuming cylindrical pore geometry. The BET surface area of the expanded graphite increased with increasing CNT loading in the 3D pillared structure (Figure S4 in the Supporting Information), indicating, once again, the efficient layer separation by the growing VACNT pillars to gain the intrinsic surface area associated with the graphene sheets. These inherently porous 3D pillared VACNT−graphene architectures with the unique conductive carbon network can be used as an effective scaffold for depositing other pseudocapacitive active materials, such as nickel hydroxide with large pseudocapacitance, to fabricate high performance supercapacitors. Nickel hydroxide is an attractive material for supercapacitor applications because of its high theoretical specific capacitance (2602.5 F/g), well-defined redox behavior, and low cost.[36] As a result of the insulating nature of $Ni(OH)_2$, however, the associated pseudocapacitors often suffer from a narrow electrochemical window, limited rate capability, and reversibility. To overcome these limitations, it is desirable to incorporate nickel hydroxide onto the 3D conductive carbon framework to ensure fast electron and ion transport. Consequently, electrochemical deposition[41] is employed in this study to produce the $Ni(OH)_2$-coated 3D pillared VACNT−graphene architectures.

Figure 5 shows SEM images of a 3D pillared VACNT (10-μm long)−graphene architecture before and after the $Ni(OH)_2$-coating, under different magnifications. A comparison of parts b and d of Figure 5 reveals a layer of uniform nickel hydroxide coating around each of the constituent VACNTs, while they

dx.doi.org/10.1021/cm2021214 |Chem. Mater. 2011, 23, 4810–4816

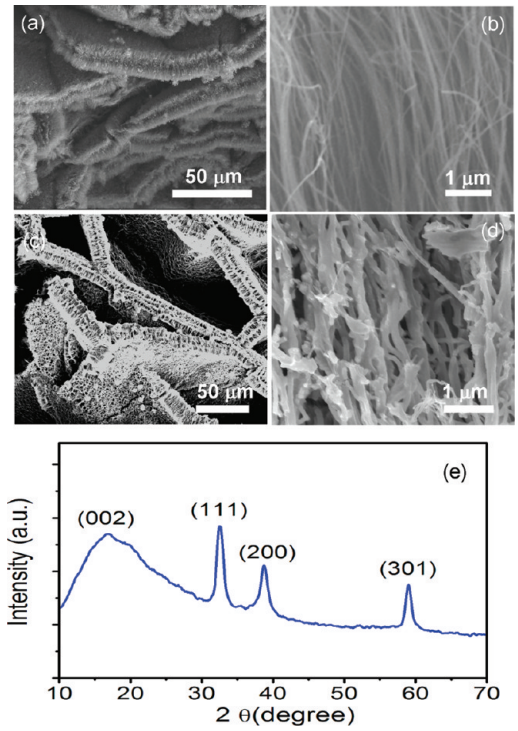

Figure 5. Typical SEM images of the 3D pillared VACNT−graphene architectures (cf. Figure 3, intercalated CNT length 10 μm): (a−b) without and (c−d) with $Ni(OH)_2$ coating and (e) XRD pattern of the $Ni(OH)_2$-coated 3D pillared VACNT−graphene composite (58 wt % $Ni(OH)_2$).

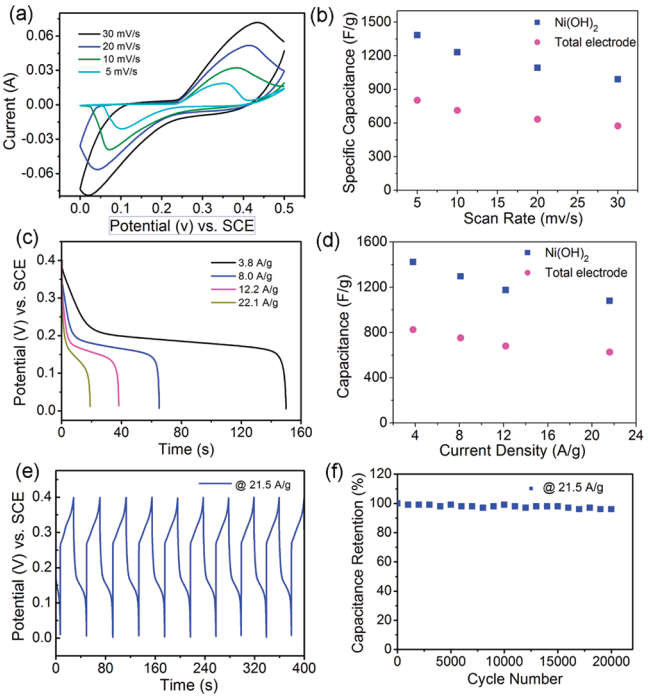

Figure 6. (a) CV curves and (b) specific capacitance (calculated from both the $Ni(OH)_2$ mass and the total electrode mass) at various scan rates for the $Ni(OH)_2$-coated VACNT−graphene electrode in an aqueous 2 M KOH. (c) Galvanostatic discharge curves of the $Ni(OH)_2$-coated VACNT−graphene electrode at various discharge current densities. (d) Average specific capacitance (calculated from both the $Ni(OH)_2$ mass and the total electrode mass) for the $Ni(OH)_2$-coated VACNT−graphene electrode at various discharge current densities. (e) Galvanostatic charge and discharge curves for the $Ni(OH)_2$-coated VACNT−graphene electrode at a current density of 21.5 A/g. (f) Average specific capacitance versus cycle number for the $Ni(OH)_2$-coated VACNT-graphene electrode at a galvanostatic charge and discharge current density of 21.5 A/g.

largely retain their vertical alignment. The presence of $Ni(OH)_2$ was further confirmed by the XRD pattern shown in Figure 5e, in which the broad peak centered at 20° corresponds to the thermally expanded graphite with all other three sharp peaks attributable to the α-$Ni(OH)_2$ structure.[40,42]

Figure 6a shows the cyclic voltammetry (CV) curves for the $Ni(OH)_2$-coated VACNT−graphene architecture (CNT length 10 μm, 58 wt % $Ni(OH)_2$) in an aqueous solution of KOH (2 M) electrolyte at the scan rates of 5, 10, 20, and 30 mV/s. As can be seen, a pair of strong redox current peaks appeared, arising from the Faradaic reactions of Ni(II) ⟷ Ni(III) associated with the $Ni(OH)_2$ coating.[36] The average specific capacitance of the $Ni(OH)_2$-coated VACNT−graphene electrode was calculated from the CV curves (see the Experimental Section for the calculation details) and plotted in Figure 6b, which shows an initial decrease with increasing scan rate from about 1384 F/g at a scan rate of 5 mV/s to 970 F/g (based on the active material, i.e., $Ni(OH)_2$) at 30 mV/s before leveling off. Even on the basis of the total electrode mass, the capacitance still reaches as high as 803 F/g at 5 mV/s. Figure 6c shows the corresponding galvanostatic discharge curves for the $Ni(OH)_2$-coated VACNT−graphene electrode at various current densities of 3.8, 8.0, 12.2, and 22.1 A/g. In a good agreement with the CV measurements, the shape of the charge−discharge curves shown in Figure 6c does not show the characteristic of an electric double layer capacitor (EDLC) but mainly pseudocapacitance. Although the VACNT−graphene framework itself could act as an EDLC (Figures S5 and S6 in the Supporting Information), a low specific capacitance of about 110 F/g at a scan rate of 10 mV/s was found for this particular VACNT−graphene architecture with unoptimized network porosity (Figure 5a) before the $Ni(OH)_2$-coating. Owing to the significant contribution from the pseudocapacitance, the $Ni(OH)_2$-coated VACNT−graphene architecture exhibited a specific capacitance as high as 1065 F/g (based on the active material) even at a current density as high as 22.1 A/g (Figure 6d), indicating great potential for high power operation.[43]

To test the electrochemical stability of the $Ni(OH)_2$-coated VACNT−graphene electrode, we performed the charge−discharge cycling at a relatively high current density of 21.5 A/g. As can be see in Figure 6e−f, there was only 4% capacity loss after 20 000 consecutive cycles, indicative of an excellent long-term electrochemical stability. Figure 6e shows also a Columbic efficiency close to 99% for each of the charge−discharge cycles. Meanwhile, we have also investigated the influence of the intercalated VACNT length in the 3D VACNT−graphene architectures on the capacitive performance after having been coated with $Ni(OH)_2$ under the same conditions, at the same charge/discharge current density of 3.8 A/g. It was found that the capacitance slightly decreased with increasing VACNT length (Figure S7 in the Supporting Information).

Figure S8 in the Supporting Information shows Nyquist plots of the electrochemical impedance spectra (EIS) of a 3D VACNT−graphene electrode before and after $Ni(OH)_2$

dx.doi.org/10.1021/cm2021214 |Chem. Mater. 2011, 23, 4810–4816

deposition. The equivalent series resistance (ESR) values obtained from the *x*-intercept of the Nyquist plot are 2.4 and 3 Ω, respectively. This magnitude is slightly smaller than that of the reported $Ni(OH)_2$ coated nickel foam electrodes with superb capacitive performance.[41] For the $Ni(OH)_2$-coated 3D pillared VACNT−graphene nanostructure, the presence of a semicircle is attributable to the charge-transfer process. Overall, the EIS results indicate, once again, that the $Ni(OH)_2$-coated 3D pillared VACNT−graphene nanostructure contributes both a fast pseudocapacitance and the EDLC.

Compared to many previously reported pseudocapacitive materials, including RuO_2,[25] MnO_2,[26] NiO,[27] Mn_3O_4,[28] and $Ni(OH)_2$[29,30] as well as their composites with CNTs or graphene,[31−36] for the state-of-the-art supercapacitors, the $Ni(OH)_2$-coated VACNT−graphene electrode exhibited a much better stable specific capacitance at high charge/discharge rates. More importantly, the $Ni(OH)_2$-coated VACNT−graphene electrode can deliver a high energy density (e.g., ∼35 Wh/kg) at a high power density (e.g., ∼8 kW/kg) (Figure S9 in the Supporting Information). Using the simplified estimation method,[44,45] the energy and power densities shown in Figure S9 in the Supporting Information were translated into the corresponding data in Figure S10 in the Supporting Information for packaged capacitors. The observed high power and energy densities, in conjunction with the high rate capability and excellent cycling stability, make the $Ni(OH)_2$-coated VACNT−graphene architectures useful for high performance supercapacitors. The observed superb electrochemical performance of the $Ni(OH)_2$-coated VACNT−graphene electrode could be attributed to their unique 3D porous structure. First, the VACNT and graphene conductive network allows for efficient charge transport. Second, the inherently porous structure, though yet optimized, could significantly facilitate the electrolyte diffusion and, hence, an enhanced ionic conductivity. Finally, the VACNT pillars with excellent mechanical properties can act as a structural support to reduce possible cycle degradation caused by possible volume changes of the nickel hydroxide coating during the redox reaction.

■ CONCLUSIONS

In summary, we have developed novel 3D pillared VACNT−graphene architectures by growing vertically aligned carbon nanotubes between graphitic layers in thermally expanded HOPGs. By controlling the fabrication process, we can tune the length of the VACNT pillars. These 3D architectures with a tunable pillar length (PL) have been further tuned through hybridization with other functional nanomaterials, such as nickel hydroxide, by a simple electrodeposition process, to demonstrate their potential applications for high-performance supercapacitors with a high rate capability and an excellent cycling ability. Apart from the demonstrated great potential as high-performance supercapacitors, these 3D pillared VACNT−graphene architectures should be also attractive for many other potential applications, including the production of new efficient electrodes for batteries and fuel cells, nanoporous structures for hydrogen/gas storages, tailored orthogonal thermal/electrical transport materials, and building blocks for nano/microscale integrated devices.

■ EXPERIMENTAL SECTION

Materials. Highly ordered pyrolytic graphite (HOPG) was purchased from SPI Supplies. Sulfuric acid and nitric acid were purchased from Fisher Scientific while iron phthalocyanine and silicon tetrachloride were purchased from Sigma-Aldrich. Compressed hydrogen and argon were supplied by Airgas Company.

Thermal Expansion and Silicon Oxide Coating of HOPG. A thin-layer of HOPG was first immersed in a H_2SO_4/HNO_3 (v/v = 3:1) mixture for a predetermined time, and then, the acid-treated graphite layer was washed three times with distilled water. After air-drying, the acid-treated graphite was put in the middle of a tube furnace to be heated up to 1000−1200 °C under a purging gas mixture of argon (300 mL/min) and hydrogen (30 mL/min) bubbling through silicon tetrachloride in an ambient atmosphere for 5 min to produce the SiO_2 coating for facilitating the growth of VACNTs.[38]

Fabrication of the 3D Pillared VACNT−Graphene Architecture. VACNTs were grown into the thermally expanded and SiO_2-coated HOPG by pyrolysis of iron phthalocyanine in a quartz tube furnace under argon/hydrogen at 800−1000 °C, according to the published procedure.[24] The length of the VACNTs in the resultant 3D pillared VACNT−graphene architectures was controlled by regulating the nanotube growth conditions (e.g., deposition time). The percentage VACNT mass loading was calculated from the mass of the intercalated VACNTs divided by the whole weight of the VACNT−graphene sample, while the VACNT mass was calculated from the weight difference of the thermally expanded HOPG before and after the intercalated VACNT growth by an analytic balance. The volume change before and after the intercalation of VACNTs was calculated from the corresponding thickness change of the HOPG sample.

Preparation of the $Ni(OH)_2$-Coated VACNT−Graphene Electrode. The $Ni(OH)_2$-coated VACNT−graphene architecture was prepared by electrochemical deposition of $Ni(OH)_2$ onto a 3D pillared VACNT−graphene structure.[41] The VACNT−graphene electrode was prepared by pasting a piece of the hybrid sample (thickness, 0.5 mm; area, 3 mm × 3 mm) on a nickel foil with graphite milk. The electrodeposition was conducted on a Chenhua CHI760 model electrochemical workstation with a three-electrode cell, consisting of a saturated calomel electrode (SCE) as the reference electrode, a platinum plate as the counter electrode, and the 3D pillared VACNT−graphene working electrode. An aqueous solution of 0.2 M $Ni(NO_3)_2$ was used as the electrolyte. Prior to the electrodeposition, the 3D pillared VACNT−graphene electrode was immersed into an aqueous 1 M HNO_3 for 10−20 min to activate the nanotube surface. The electrodeposition was then carried out at a constant potential of −0.85 V versus SCE. To deposit a $Ni(OH)_2$ film of about 0.4 mg, the corresponding deposition charge quantity is approximately 0.67 C, which was estimated by Faraday's law. After deposition, the as prepared composite was washed with water several times and used in situ as the electrode for subsequent capacitance measurements.

Electrochemical Measurements. A three-electrode cell with a SCE electrode and Pt wire as the reference and counter electrodes, respectively, was employed for electrochemical measurements of the 3D pillared VACNT−graphene electrode before and after hybridization with $Ni(OH)_2$. The measurements were carried out on a CHI electrochemical workstation in a 2 M KOH aqueous electrolyte at room temperature.

The specific capacitance of the electrode was calculated from CV curves according to the following equation:

$$C = \frac{1}{\omega v (V_c - V_a)} \int_{V_a}^{V_c} I(V)\, dV \qquad (1)$$

where C is the specific capacitance (F/g), ω is the mass of electroactive materials in the electrode (g), v is the potential scan rate (mV/s), V_c and V_a are the integration limits of the voltammetric curve (V), and $I(V)$ denotes the response current density (A). Energy density (E) was derived from the CV curves using the following equation: $E = 0.5\, C\Delta V^2$, where C is the specific capacitance of the active material, and ΔV is the

voltage range of one sweep segment. Power density (P) was calculated from the following equation: $P = E/\Delta t$, where E is the energy density and Δt is the time for a sweep segment. The active materials used for all the calculations include the VACNT−graphene framework.

Characterization. The morphology and structures were characterized with a SEM instrument (NOVA NANOSEM 600) operated at 5.0 kV and a TEM instrument (FEI Titan 80-300). Raman spectroscopy was performed by using a Renshaw InVia Raman spectrometer with 514.5 nm excitation. XRD data was collected on a Rigaku X-ray diffractometer. Brunauer−Emmet−Teller (BET) specific surface area was determined from N_2 adsorption by using an IGA intelligent gravimetric analyzer (HIDEN ISOCHEMA) at liquid nitrogen temperature.

■ ASSOCIATED CONTENT

Supporting Information. TEM images, Raman spectra, nitrogen adsorption isotherm, CV curves, specific capacitance, and Nyquist and Ragone plots. This material is available free of charge via the Internet at http://pubs.acs.org.

■ AUTHOR INFORMATION

Corresponding Author

*E-mail: liming.dai@case.edu; ajit.roy@wpafb.af.mil.

Author Contributions

§These authors contributed equally to this work.

■ ACKNOWLEDGMENT

The authors acknowledge the financial support from the AFOSR (FA 9550-10-1-0546) and MURI project under Low Density Materials Program (Dr. Joycelyn Harrison, Program Manager).

■ REFERENCES

(1) Novoselov, K. S.; Geim, A. K.; Morozov, S. V.; Jiang, D.; Zhang, Y.; Dubonos, S. V.; Grigorieva, I. V.; Firsov, A. A. *Science* **2004**, *306*, 666.
(2) Park, S.; Ruoff, R. S. *Nat. Nanotechnol.* **2009**, *4*, 217.
(3) Li, X. S.; Cai, W. W.; An, J. H.; Kim, S.; Nah, J.; Yang, D. X.; Piner, R.; Velamakanni, A.; Jung, I.; Tutuc, E.; Banerjee, S. K.; Colombo, L.; Ruoff, R. S. *Science* **2009**, *324*, 1312.
(4) Li, D.; Muller, M. B.; Gilje, S.; Kaner, R. B.; Wallace, G. G. *Nat. Nanotechnol.* **2008**, *3*, 101.
(5) Liu, Z. F.; Liu, Q.; Huang, Y.; Ma, Y. F.; Yin, S. G.; Zhang, X. Y.; Sun, W.; Chen, Y. S. *Adv. Mater.* **2008**, *20*, 3924.
(6) Wang, X.; Zhi, L. J.; Mullen, K. *Nano Lett.* **2008**, *8*, 323.
(7) Yu, D. S.; Dai, L. M. *J. Phys. Chem. Lett.* **2010**, *1*, 467.
(8) Yoo, E.; Kim, J.; Hosono, E.; Zhou, H. S.; Kudo, T.; Honma, I. *Nano Lett.* **2008**, *8*, 2277.
(9) Qu, L. T.; Liu, Y.; Baek, J. B.; Dai, L. M. *ACS Nano* **2010**, *4*, 1321.
(10) Yu, D. S.; Yang, Y.; Durstock, M.; Baek, J. B.; Dai, L. M. *ACS Nano* **2010**, *4*, 5633.
(11) Gong, K. P.; Du, F.; Xia, Z. H.; Dustock, M.; Dai, L. M. *Science* **2009**, *323*, 760.
(12) Qu, L. T.; Du, F.; Dai, L. M. *Nano Lett.* **2008**, *8*, 2682.
(13) Sun, Y.; Wu, Q.; Shi, G. *Energy Environ. Sci.* **2011**, No. 4, 1113–1132.
(14) Frackowiaka, E.; Béguin, F. *Carbon* **2002**, *40*, 1775.
(15) Varshney, V.; Patnaik, S. S.; Roy, A. K.; Froudakis, G.; Farmer, B. L. *ACS Nano* **2010**, *2*, 1153.
(16) Dimitrakakis, G. K.; Tylianakis, E.; Froudakis, G. E. *Nano Lett.* **2008**, *8*, 3166.
(17) Mao, Y. L.; Zhong, J. X. *New J. Phys.* **2009**, *11*, 093002.
(18) Sheka, E. F.; Chernozatonskii, L. A. *J. Comput. Theor. Nanos.* **2009**, *7*, 1814.
(19) Arellano, J. S. J. *Nano Research* **2009**, *5*, 201.
(20) Fan, Z.; Yan, J.; Zhi, L.; Zhang, Q.; Wei, T.; Feng, J.; Zhang, M.; Qian, W.; Wei, F. *Adv. Mater.* **2010**, *22*, 3723.
(21) Zhang, L. L.; Xiong, Z.; Zhao, X. S. *ACS Nano* **2010**, *4*, 7030.
(22) Su, Q.; Liang, Y. Y.; Feng, X. L.; Mullen, K. *Chem. Commun.* **2010**, *46*, 8279.
(23) Paul, R. K.; Ghazinejad, M.; Penchev, M.; Lin, J.; Ozkan, M.; Ozkan, C. S. *Small* **2010**, *6*, 2309.
(24) Huang, S. M.; Dai, L.; Mau, A. W. H. *J. Phys. Chem. B* **1999**, *103*, 4223.
(25) Jang, J. H.; Kato, A.; Machida, K.; Naoi, K. *J. Electrochem. Soc.* **2006**, *153*, 321.
(26) Chen, S.; Zhu, J.; Han, Q.; Zheng, Z.; Yang, Y.; Wang, X. *Cryst. Growth Des.* **2009**, *9*, 4356.
(27) Yuan, C.; Zhang, X.; Su, L.; Gao, B.; Shen, L. *J. Mater. Chem.* **2009**, *19*, 5772.
(28) Nagarajan, N.; Humadi, H.; Zhitomirsky, I. *Electrochim. Acta* **2006**, *51*, 3039.
(29) Patil, U. M.; Gurav, K. V.; Fulari, V. J.; Lokhande, C. D.; Joo, O. S. *J. Power Sources* **2009**, *188*, 338.
(30) Lang, J.; Kong, L.; Wu, W.; Liu, M.; Luo, Y. J. *Solid State Electrochem.* **2009**, *13*, 333.
(31) Wang, Y.; Zhitomirsky, I. *Langmuir* **2009**, *25*, 9684.
(32) Nam, K.; Kim, K.; Lee, E.; Yoon, W.; Yang, X.; Kim, K. *J. Power Sources* **2008**, *182*, 642.
(33) An, G.; Yu, P.; Xiao, M.; Liu, Z.; Miao, Z.; Ding, K.; Mao, L. *Nanotechnology* **2008**, *19*, 275709.
(34) Zhang, H.; Cao, G.; Wang, Z.; Yang, Y.; Shi, Z.; Gu, Z. *Nano Lett.* **2008**, *8*, 2664.
(35) Bi, R.; Wu, X.; Cao, F.; Jiang, L.; Guo, Y.; Wan, L. *J. Phys. Chem. C* **2010**, *114*, 2448.
(36) Wang, H.; Casalongue, H. S.; Liang, Y.; Dai, H. *J. Am. Chem. Soc.* **2010**, *132*, 7472.
(37) Yu, A.; Ramesh, P.; Itkis, M. E.; Bekyarova, E.; Haddon, R. C. *J. Phys. Chem. C* **2007**, *111*, 7565.
(38) Qu, L.; Zhao, Y.; Dai, L. *Small* **2006**, *2*, 1052.
(39) Zhang, Q.; Xu, Y.; Wang, X. *Mater. Chem. Phys.* **2004**, *86*, 293.
(40) Wu, Y.; Wang, B.; Ma, Y.; Huang, Y.; Li, N.; Zhang, F.; Chen, Y. *Nano Res.* **2010**, *3*, 661.
(41) Yang, W.; Xu, C.; Li, H. *Chem. Commun.* **2008**, 6537.
(42) Han, T. A.; Tu, J. P.; Wu, J. B.; Yuan, Y. F.; Li, Y. *Solid State Phenom.* **2007**, *121*, 1265.
(43) Zhang, H.; Cao, G.; Wang, Z.; Yang, Y.; Shi, Z.; Gu, Z. *Nano Lett.* **2008**, *8*, 2664.
(44) Mastragostino, M.; Arbizzani, Z. C.; Paraventi, R.; Zanellia, A. *J. Electrochem. Soc.* **2000**, *147*, 407.
(45) Lu, W.; Hartman, R.; Qu, L.; Dai, L. *J. Phys. Chem. Lett.* **2011**, *2*, 655.